Author Manuscript

Title: Impact of Electrolyte Composition on Bulk Electrolysis of Furfural over Platinum Electrodes

Authors: Joseph Hasse; Marc Manyé Ibáñez; Adam Holewinski

To be cited as: 10.1002/cctc.202300988

Link to VoR: https://doi.org/10.1002/cctc.202300988

Impact of Electrolyte Composition on Bulk Electrolysis of Furfural over Platinum Electrodes

Joseph C. Hasse[1,2,+], Marc Manyé Ibáñez[1,2,+], and Adam Holewinski[1,2,*]
[1]*Department of Chemical and Biological Engineering, University of Colorado, Boulder, Colorado 80309, United States*
[2]*Renewable and Sustainable Energy Institute, University of Colorado, Boulder, Colorado 80309, United States*
[+] These two authors contributed equally to this work.
[*] *adam.holewinski@colorado.edu, Phone: 303-492-3153*

Abstract

Partial oxidation of furanic biomass derivatives such as furfural is of interest for the sustainable production of chemicals including furoic acid, maleic acid, and 2,5-furandicarboxylic acid (FDCA). The oxidative bulk electrolysis of furfural is here investigated on platinum electrodes in acidic media. The effects of potential, concentration, pH, and supporting anion are studied, and selectivity trends are coupled with attenuated total reflectance surface-enhanced infrared absorption spectroscopy (ATR-SEIRAS) to illuminate adsorbate structures that influence the catalysis. Increasing potential is found to shift selectivity from primarily C_5 products to C_4 products, coincident with oxidation of the Pt surface. Selectivity changes are also observed moving from pH 1 to pH 4, with an increase in C_5 products at higher pH. Changing from the weakly adsorbing perchlorate anion to the specifically-adsorbing phosphate anion results in a number of changes that manifest differently depending on potential and pH. Selectivity to furoic acid is found to be highest above the pKa of phosphoric acid due to the strongly adsorbed phosphate ions suppressing flat-lying configurations of furfural that lead to C-C cleavage. These results point toward opportunities to use electrolyte engineering to tune selectivity and optimize surface conditions to disfavor binding of inhibitory products.

Introduction

Due to the environmental, economic, and societal pressures being generated by the use of finite fossil resources, a focus on renewable sources of energy and carbon has risen in recent decades.[1] While many renewable electricity sources have been developed[2], breakthroughs in carbon-neutral sourcing of commodity and fine chemicals—e.g., from biomass—are lacking. Difficult-to-decarbonize sectors such as aviation and heavy transport also prompt a near-term need for sustainable carbon-based fuels.[3–5] Most of the common processing techniques for the formation of these compounds from raw biomass, however, generate aqueous streams at low pH, which can be challenging to accommodate with downstream chemical conversion approaches. Additionally, aqueous reforming methods for nongaseous biomass feedstock products often require costly separation methods to achieve high purity products.[6–12] Electrochemistry is another possible approach, as it is amenable to aqueous, acidic conditions and offers some other potential advantages over traditional thermal catalysis; these include the ability to generate oxidative and reducing equivalents *in situ*, not needing to alkalize or otherwise treat the aqueous feedstock to adjust pH, as well as operating at ambient pressures and temperatures.[13–16]

Furanic derivatives, such as furfural and 5-hydroxymethylfurfural (HMF), have been identified as biomass molecules suitable to be used as a feedstock for a variety of fuels and chemicals. From these platforms, many “drop in” biofuel targets can be produced through reductive processes including hydrogenation and hydrodeoxygenation.[13, 17–21] Alternatively, a number of commodity and fine chemicals can be generated through partial oxidation of furanics.[1, 17, 22–24] Several of these

compounds have the potential to displace large petrochemical markets, and the coupled economics of (high-margin) bio-derived chemicals with (low-margin) biofuels are widely recognized as a key to making biofuels affordable. HMF has a particularly large potential market, as the oxidation product 2,5-furandicarboxylic acid (FDCA) can be used to produce polyethylene furoate (PEF), a possible green alternative to polyethylene terephthalate (PET).[25, 26] Also of interest is the partial oxidation of furfural, summarized in Figure 1, where key products include furoic acid (FA), 5-hydroxy-2(5H)-furanone (HFN), and maleic acid (MA). FA has uses as a preservative, fungicide, and pharmaceutical precursor.[27, 28] Potential routes to further carboxylation of FA to FDCA have additionally been shown, meaning that furfural may supplement HMF for PET replacements.[25, 26] HFN is used as a feed stock for multiple pharmaceutical compounds, rubber additives and agrochemical formulations.[17, 29] MA is typically produced for resins, flavorings and various Diels-Alder synthesis[17, 30–35]

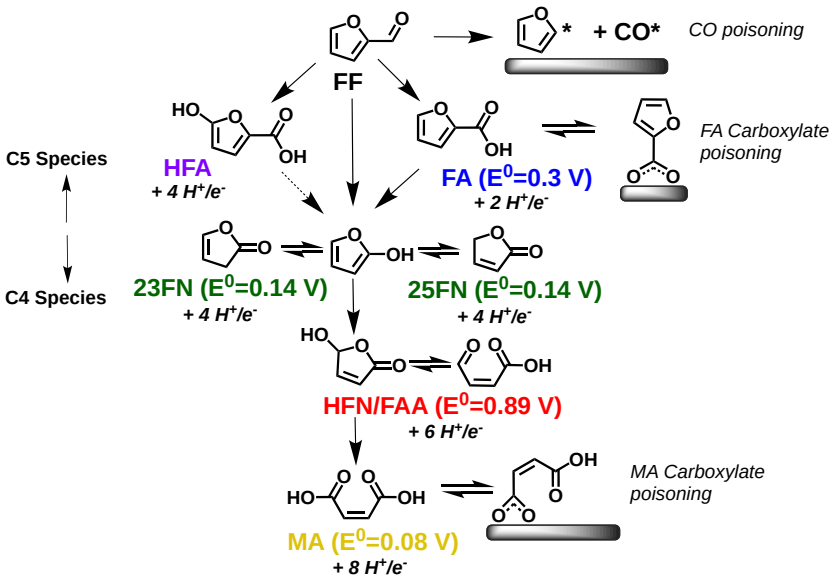

Figure 1: Schematic of routes for furfural electro-oxidation with standard potentials for major products and common bottlenecks from adsorbed carboxylates.

Our group has performed several studies on the partial oxidation of furfural.[36–38] However, these have been limited to kinetic studies at differential conversion and complimentary *in situ* attenuated total reflectance Fourier transform infrared (ATR-FTIR) spectroscopy, also in the presence of pure reactants. These studies identified the onset of steady state oxidation (~0.9 V vs. RHE) to be associated with charge transfer steps outrunning the rate of aldehyde C-C bond cleavage, which forms carbon monoxide (CO) by decarbonylation of the furfural aldehyde group (Figure 1). A slate of products, as outlined in Figure 1, were also identified: FA, MA, HFN, 2-furanones (FN) (isomers from furanol), and hydroxyfuroic acid (HFA)[36, 37]. While the standard redox potentials associated with these products serve as valuable reference points for which species are thermodynamically accessible under various conditions, the selectivity trends are not directly predicted by these potentials, and thus the need to characterize the kinetics at the level of elementary steps is underscored. Our FTIR surface investigation[38] showed several features of the reaction network that converge, regardless of the intermediate species starting point, toward accumulation of carboxylates (e.g., furoate and maleate) as strongly adsorbed surface species. Reactants and intermediates with aldehyde groups—even those forming through minority isomers such as the HFN isomer formyl acrylic acid (FAA)—were also found to decarbonylate in a chemical pathway that causes CO-poisoning at low potentials. Despite the mechanistic insights from these studies, however, their limitation to very low conversion and a narrow regime of reaction conditions (high concentration, low pH) restricts the applicability toward understanding how to

optimize bulk electrolysis. The present work characterizes product distributions and the influence of surface adsorbates across a broader range of reaction environments (pH, electrolyte ions) at higher conversions.

Results & Discussion

Cyclic Voltammetry Characteristics

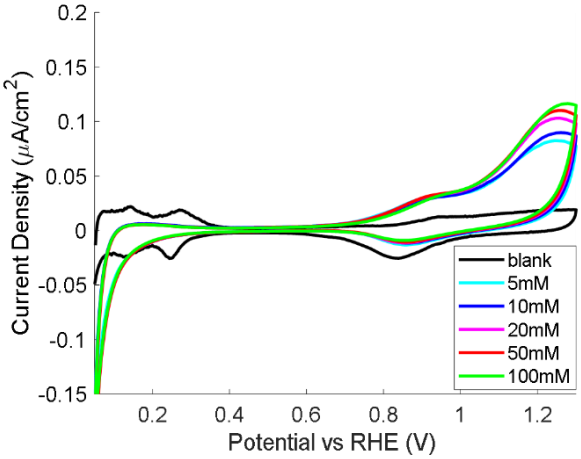

Figure 2: Cyclic voltammograms in varying concentrations of furfural from 0 to 100 mM, taken at 20 mV/s on a Pt plate electrode in 0.1 M $HClO_4$.

The electrochemical features of furfural on Pt are shown using cyclic voltammetry at varying concentrations in Figure 2. After the addition of furfural, the hydrogen absorption features of platinum are suppressed and a cathodic current can be seen starting at ~0.1 V, consistent with previous reports.[36] Furfural oxidation features are seen to the anodic side of the scan beginning just below ~0.8 V; At higher potentials, higher concentrations give higher currents, indicative of a small positive reaction order. The potential-dependence of the current is also positive but weak (far from exponential as in Butler-Volmer kinetics). These behaviors together are consistent with the accumulation of strongly bound intermediates approaching saturation of the surface and a significant

degree of rate control by a chemical (i.e., non-charge-transfer) process. In our previous spectroscopic work,[39] we observed that many surface-bound carboxylates, such as furoate and maleate, tend to accumulate and have slower rates of desorption or breakdown than other products such as the furanones. Given that the concentration and potential dependencies are still non-zero, it is possible that some electrochemical steps shift their equilibria to promote subsequent chemical steps by raising relevant adsorbed precursor concentrations. Selectivity toward deeper oxidation products (representing more electrons passed per furfural molecule converted) also increases at higher potentials and thus can show higher currents for a given rate of turnover.

Reaction Trends with Time and Potential

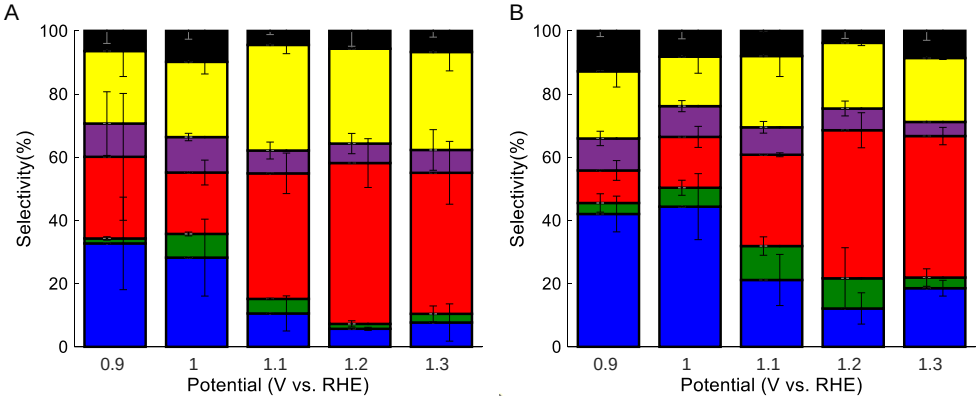

Figure 3: Selectivities to FA (blue), FN (green), HFN (red), HFA (purple), MA (yellow) and unquantified (mostly CO_2) (black) given across a range of potentials and two concentrations (10 mM (A) and 50 mM (B)) after 22 hours of electrolysis.

The product distribution from furfural oxidation over Pt/C was compared across operating potentials at two concentrations (10 and 50 mM) during extended electrolysis (with an additional concentration available in Figure S1). We investigated a potential window between 0.9 and 1.3 V and identified FA, FN, HFN, HFA, MA, and CO_2 as products. No new products were identified relative to previous differential conversion experiments.[36] Selectivities are shown in Figure 3, and a full compilation of metrics

including conversions, faradaic efficiencies, individual product yields and carbon balances is provided in Tables S1-2. Faradaic efficiencies to the C_4 and C_5 products were generally above 70%, with conversion ranging from 40-80%, generally rising with potential.

We note that due to a lack of any detectable C_1-C_3 species or oligomeric coupling products—per examination with MS, UV, and RID detection in liquid chromatography, as well as NMR—CO_2 is ascribed to both the formation of the detected C_4 products and to a separate total oxidation pathway, as has been previously proposed[36]. CO_2 could not accurately be directly quantified due to aqueous carbonate equilibrium coupled with an overall very low rate of production and uncertain losses in headspace gas during repeated time-point samples. As such, the portion of selectivity marked in black in Figure 3 (and all subsequent figures) corresponds to what we believe is a large majority CO_2 generated by total oxidation but could contain other low yields of undetected products. For best estimation purposes, charge not accounted for with C_4-C_5 products was ascribed to the total oxidation path to CO_2 (after confirming that support breakdown and oxygen evolution were also negligible). Comparable observations of a total oxidation path have been made with similar molecules (namely for furan[40] and benzaldehyde[41]) on platinum electrodes under similar conditions. Some loss of furfural was also noted due to incorporation into the Nafion 117 membrane itself during crossover, but control experiments indicated this should not be more than a few percent of the carbon balance.

In both the 10 mM and 50 mM electrolyses, a distinct change in selectivity is observed from 1 to 1.1 V, correlated with the well-established transition from predominantly metallic Pt to a surface PtO_x phase. Prior to this transition, FA (the only 2

e⁻ product) is dominant, with small amounts of the deeper oxidized HFN, HFA and MA also present. After the transition, selectivity toward FA decreases, with larger amounts of HFN and MA (6 and 8 e⁻, respectively) contributing to the balance. In all cases, the conversion (and correspondingly, the charge passed) over the course of the experiment increases with increasing potential. Differences in the 10 mM and 50 mM experiments are also evident. The higher concentration gives a larger proportion of FA (less HFN and MA) at all potentials. This suggests that the pathway to higher oxidized species may be facilitated by a decrease in surface furfural concentration. A larger furfural concentration on the surface may increase the degree of favorable interactions with aromatic species, particularly stabilizing strongly adsorbed carboxylates such as furoate and promoting formation of FA as a product. Similar shifts in selectivity have been observed to be even more pronounced for furfural oxidation on Au electrodes, where C-C activation is slow and C_4 products are almost entirely suppressed at higher furfural concentrations.[37] The less dramatic shift observed here can be explained by the more active nature of platinum (allowing for C_4 products at lower overpotentials).

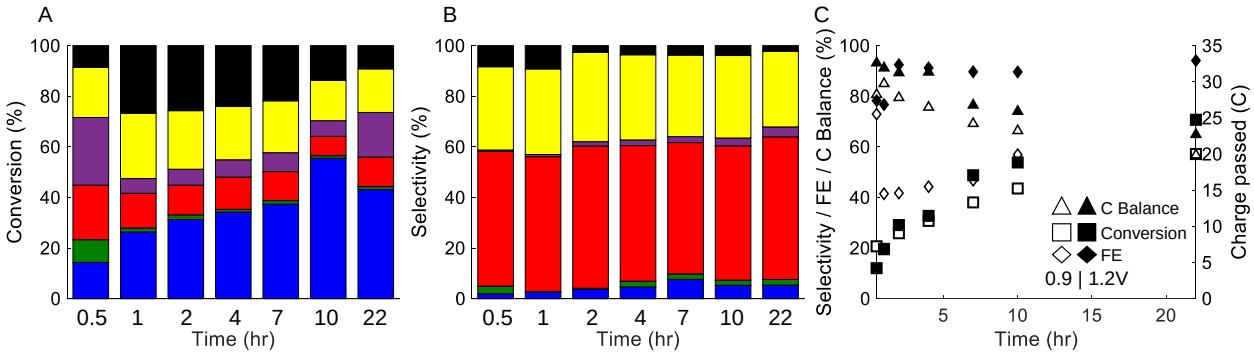

Figure 4: Selectivities to FA (blue), FN (orange), HFN (red), HFA (purple), MA (yellow) and unquantified (mostly CO_2) given for 0.9 V and 1.2 V (A/B respectively) over 22 hours of electrolysis for 10 mM FF. In panel C, total faradic efficiency (diamonds), furfural conversion (squares), and carbon balance (triangles) are also given.

Regardless of the slight differences between the high and low concentration cases, the dominant feature of the product distribution is the potential dependence. To examine how the product distributions evolve at each potential, we next focus in Figure 4 on a comparison of product distribution vs. time at two representative potentials (0.9 V and 1.2 V) (additional metrics in Tables S3-4). Simultaneous to the reaction progress at both potentials is an increase in FA selectivity with time (albeit a minor product at 1.2 V). This is accompanied by the highest observed C_4 product selectivities appearing at the initial half-hour time point for both potentials and steadily decreasing with time. Considering past spectroscopic studies showing high affinity of Pt for FA[39], we infer that the selectivity trends are likely due to favorable adsorbate-adsorbate interactions (e.g., pi-stacking) with surface-bound FA, which can readsorb and promote selectivity towards more FA, albeit with suppression of rate. Accumulation of MA at higher potential may also have a similar though less effective role in driving production of FA since site blocking can decrease the likelihood of rings reaching flat-lying conformations that promote C-C cleavage, irrespective of more specific interactions such as pi-stacking.[42–44] Interestingly, the furfural conversion at both potentials does not differ dramatically (within 15%). This may also support the argument that the system is limited, both at high and low potentials, by carboxylate removal from the surface.

While, as should be expected, the conversion increases asymptotically over time in each case, it is also notable that the conversion halts with significant remaining furfural. This apparently relates to a catalyst deactivation process. Fouling from coking or polymerization are possible, but we find that these pathways are minimal, unlike what has been documented in alkaline conditions[45]. Instead, we find that deactivation relates to

the accumulation of strongly bound product species. To illustrate this, we performed a recycle study, reusing catalysts after only rinsing with blank electrolyte. We found that a majority of the lost current is regained—about 70% activity retention is observed relative to time zero on the initial run. We thus conclude that while some of the loss is due to permanent deactivation of catalyst, most of the suppression in current seen during electrolysis is simply product inhibition. Permanent losses are most likely via known degradation mechanisms for Pt/C, such as particle ripening and mechanical detachment of the catalyst, rather than coking or polymers encapsulating the particles.

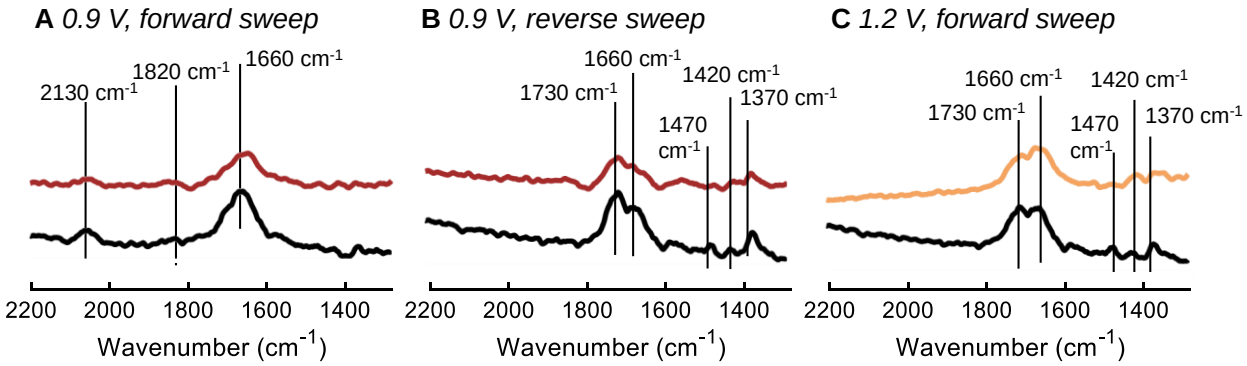

Figure 5: ATR-SEIRA spectra for simulated 22 hr reaction mixtures (50 mM) compared to pure furfural in 0.1 M $HClO_4$ on a Pt film. Spectra were taken at a scan rate of 1 mV/s, summing 150 interferograms over 100 s for each 100 mV increment and are presented at 0.9 V on both the forward and reverse sweep (A and B) as well as at 1.2 V (C). Colors: reaction mixture at 0.9 V (maroon) and 1.2 V (tan); furfural under same conditions (black).

To further interrogate the effects of time and potential on the electrode surface, *in situ* ATR-SEIRA spectroscopy was performed on mixtures that were formulated to match the late (22 hour) electrolysis solution compositions at both 0.9 V and 1.2 V (Figure 5). We have previously studied the fresh furfural system and individual products intensively[39] and will thus only provide a brief overview of the overall spectral features when comparing the specific reaction mixtures here. Comparisons are presented at the

same potentials as the electrolyses in Figure 4, although spectra for each mixture were measured during a slow scan (1 mV/s) across a range of potentials because different moieties can have revealing signatures under different conditions (full potential series of spectra in SI Figures S2-4). Prior to onset of reaction, the main aldehyde stretch of furfural is seen at 1660 cm^{-1}, alongside adsorbed CO (from a decarbonylation pathway of adsorbed furfural) giving linear and bridge-bound (CO_L and CO_B) stretches at 2030 cm^{-1} and 1820 cm^{-1} respectively.

Comparing the fresh furfural (black) to the 0.9 V (forward sweep) 22 hr reaction mixture in Figure 5A (maroon), a slight broadening of the carbonyl peak can be detected. This is due to the contribution of other carboxylic acids and lactone products (FA/MA and FN/HFN respectively) contributing intensity in the carbonyl region. In Figure 5B, we present the same conditions as Figure 5A, after sweeping up to 1.3 V and reversing back to 0.9 V. At this point, the residual CO is cleared, and a broad carbonyl peak with its highest intensity at 1730 cm^{-1} takes precedence. The furfural peak loses intensity in the reaction mixture—relative to bulk furfural—and appears more weakly as a shoulder aside the 1730 cm^{-1} peak. In addition, a slight shoulder around 1620 cm^{-1} is also clear. We have previously observed this feature from pure HFN and MA and suggested it to be evidence of the ring-opened isomer of HFN (specifically, FAA) or an intermediate in the transformation of HFN to MA[39]. By contrast, this feature is overshadowed in pure furfural by the furfural aldehyde peak. Additionally, we observe growth of 3 peaks at lower wavenumbers (1470,1420 and 1370 cm^{-1}). The first two peaks can be attributed to ring stretches of bound furoate, while the last (1370 cm^{-1}) is a bound carboxylate stretch that can correspond to either/both furoate and maleate. As these peaks all show

approximately the same ratios of intensity as in the pure bulk furfural spectra, it can be suggested that approximately the same ratio of FA to MA exists on the surface as the reaction progresses to higher conversion.

In Figure 5C, we compare fresh furfural (black) to the 1.2 V, 22 reaction mixture (tan). The forward and reverse sweeps are virtually identical so for brevity only the forward is presented. Interestingly, at 1.2 V the carbonyl region of the mixture does not exhibit nearly as much intensity at higher wavenumbers (1730 cm^{-1} feature) as it does at 0.9 V. Further, the lower wavenumber peaks (1470,1420 and 1370 cm^{-1}) do not appear in the same ratios as the fresh furfural case (unlike what is seen at 0.9 V). While all of these features diminish to some extent, the 1370 cm^{-1} peak, which can be attributed to either bound maleate or furoate, diminishes most significantly. Since the peaks at 1470 and 1420 cm^{-1} are associated with furoate, the decrease at 1370 cm^{-1} must be due to a very low population of MA bound as a carboxylate. Considering that MA is a major product at 1.2 V, this may indicate that MA is less strongly bound to the oxidized Pt surface than FA (perhaps due to less favorable adsorbate-adsorbate interactions than FA).

Electrolyte and pH Effects

Additional studies were carried out to understand the influence of the electrolyte solution environment on furfural oxidation. Figure 6A compares cyclic voltammograms of 100 mM furfural in several different electrolyte solutions, with corresponding electrolysis results given in Figure 6B. Conditions below and above the pKa of the relevant carboxylic acids (pH 1 and pH 4) were explored using both non-adsorbing ClO_4^- as well as $H_2PO_4^-$, which is well-documented to specifically adsorb across major crystal facets of Pt.[46, 47] Inspecting the CVs, the most notable effect of increasing pH (all other factors equal) is

observed to be a later onset and lower maximum current than lower pH. When switching anion from phosphate to perchlorate, the changes in onset of reaction are more subtle, but an inflection occurs in the perchlorate systems leading to a small plateau in current at ~0.8 V (pH 1) and at ~1 V (pH 4) respectively. This is much less pronounced in the phosphate systems (completely suppressed at pH 4) and likely is a result of the competitive adsorption of phosphate with furfural and hydroxide. Due to the presence of furfural, as well as the convolution of various facets on polycrystalline Pt, overlap of OH* adsorption features, and uncertain adsorption valency of the phosphate species, we do not attempt to quantify the phosphate coverage, but focus on its qualitative role.

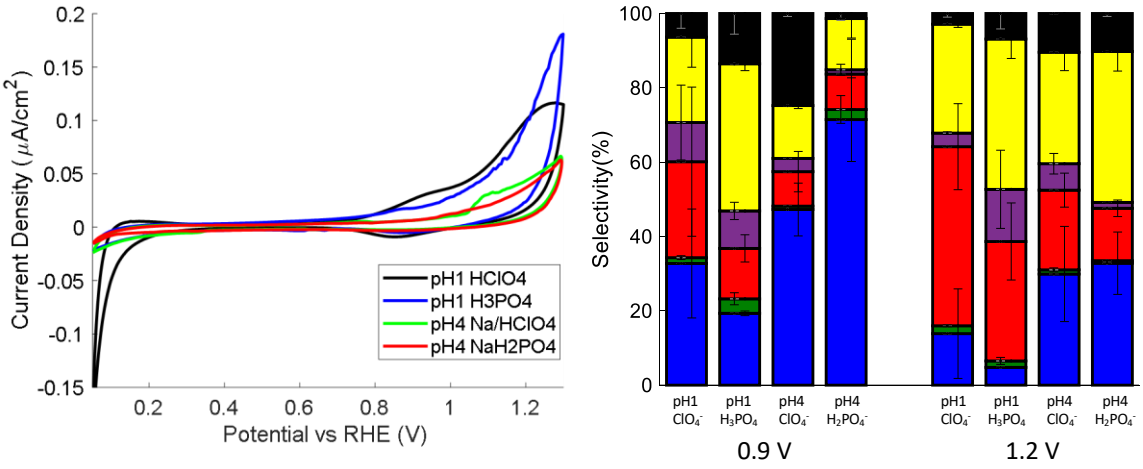

Figure 6: (A) Cyclic voltammograms using 100 mM FF in 0.1 M $HClO_4$ (black), 1.3 M H_3PO_4 (cyan), 0.001 M $HClO_4$ + 0.099 M $NaClO_4$ (red), 1 M NaH_2PO_4 (green) on a Pt plate electrode at 20 mV/s. (B) Selectivities to FA (blue), FN (orange), HFN (red), HFA (purple), MA (yellow) and unquantified (mostly CO_2) (black) at 0.9 V and 1.2 V, at both pH 1 and pH 4. 1 M phosphate or perchlorate anion concentration was maintained in each case and electrolysis run for 22 hours in 10 mM FF.

Comparing electrolyses (Figure 6B) (additional metrics in Table S6), it is observed that when shifting to pH 4 and retaining ClO_4^- as the supporting anion, there is an increase in the FA selectivity, mainly at the expense of HFN. While selectivity favors FA at lower

potential, the *change* in selectivity is more pronounced at 1.2 V than at 0.9 V. This could perhaps be due to the deprotonation of furoic acid at elevated pH causing it to be drawn more strongly to the electrode surface at higher potential, resulting in moderately better suppression of binding configurations of furfural that would promote C_4 products.

When phosphate (H_3PO_4/NaH_2PO_4) is used as the supporting anion instead of perchlorate, different behaviors are seen depending on the pH and potential. Selectivity toward FA is enhanced at pH 4, most significantly at 0.9 V. The selectivity to FA reaches over 70% at this condition, likely as a result of the adsorbed phosphate interfering with the ability of ring structures to lie flat on the surface and access C-C cleavage paths. In contrast, selectivity to FA decreases in phosphate at pH 1, where selectivity toward MA increases. At low pH and elevated potential (1.2 V) the MA is produced at the expense of FA, while at high pH the MA comes more at the expense of HFN.

We speculate that the differences in the influence of phosphate are likely due to the form phosphate ions prefer at the pH conditions selected. At low pH, phosphates mainly exist as protonated phosphoric acid H_3PO_4 and will be less prone to specific adsorption than dihydrogen phosphate ($H_2PO_4^-$), dominant at pH 4. We posit that at lower pH, phosphate species interact enough with the surface to break up the pi-pi interactions that encourage upright binding of furfural, but not enough to suppress flat-lying configurations. Since flat-lying configurations of furfural are necessary to access C-C cleavage and therefore C_4 products, disruption of favorable adsorbate-adsorbate interactions would naturally lead to higher MA production. On the other hand, dominant specific adsorption of phosphates at high pH could lead to a situation that preserves selectivity toward FA by leaving only a small portion of available sites that furfural must

bind to upright. In the absence of other nearby furoates, the FA could also desorb quickly, leading to the high selectivity observed. The steering effects of specifically-adsorbed phosphate may then again become diminished at higher voltage, assuming weaker binding to the surface oxide of Pt.

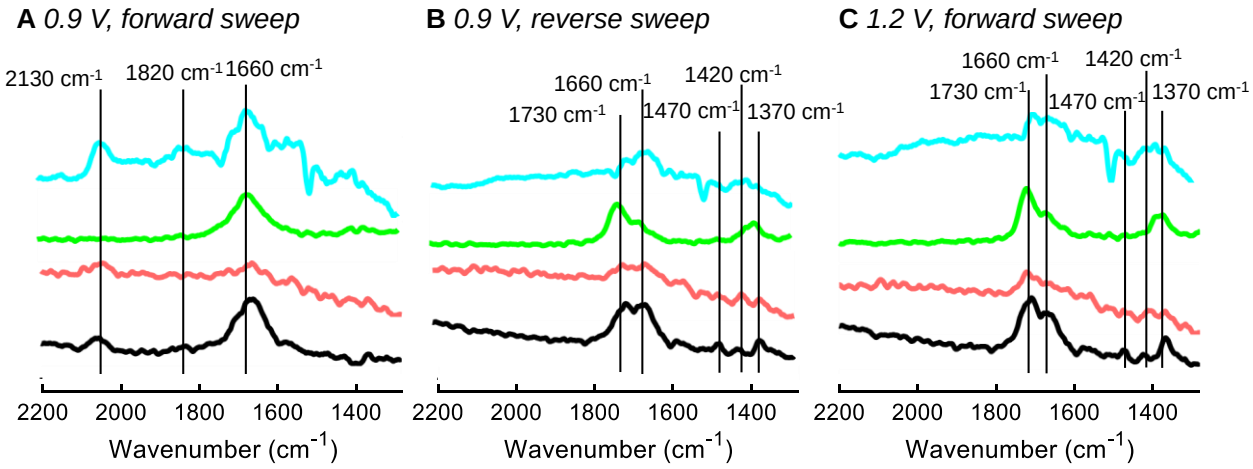

Figure 7: ATR SEIRA spectra for the electro-oxidation of 100 mM furfural in 0.1 M HClO4 (black), 0.001 M $HClO_4$ + 0.099 M $NaClO_4$ (red), 1M H_3PO_4 (cyan) and 1M NaH_2PO_4 (green) on a Pt film. Spectra are taken at a scan 1 mV/s summing 150 interferograms over 100 s for each 100 mV increment, however, only the 0.9V spectra from the forward and reverse sweep (A and B) and 1.2 V (C forward sweep are presented.

To attempt to further rationalize the differences in selectivity with pH and electrolyte ion, we again explore the state of the Pt surface under reaction conditions with ATR-SEIRAS. In Figure 7, we show spectra at 0.9 V during a slow (1 mV/s) scan in both forward and reverse sweeps, as well as forward sweeping spectra at 1.2 V (full potential series of spectra in SI Figures S5-S7). It can firstly be noted that, in all of the conditions except pH 4 phosphate (green), the surface initially shows adsorbed CO at 0.9 V on the forward sweep. Besides having no signs of CO poisoning, the pH 4 phosphate shows only evidence of adsorbed furfural and no evidence of early formation of C_4 or C_5 oxidation products. This supports the idea that furfural is unable to adopt flat-lying geometries in pH 4 phosphate. Nonetheless, on the reverse sweep, all of the electrolytes (including pH

4 phosphate) show features in the 1730-1700 cm^{-1} range associated with higher energy carbonyl groups of various products (carboxylic acids and lactones). The three lower wavenumber features noted previously to correspond with ring features and the surface carboxylate stretch (1470,1420 and 1370 cm^{-1}) also appear in each electrolyte, except pH 4 phosphate, where only the 1370 cm^{-1} carboxylate feature (believe to correspond with bound MA) appears after accessing higher potentials. This would suggest that maleate is a more prominent spectator than furoate under the conditions that are selective to FA product (lower organic coverage imposed by adsorbed electrolyte).

At the higher potential (1.2 V spectra), the pH 4 phosphate electrolyte does not strongly exhibit the main furfural 1660 cm^{-1} feature, which decays almost entirely in favor of the 1730 cm^{-1} product peak. Depletion of adsorbed furfural under these conditions is likely due to competition by the attraction of deprotonated carboxylic acids (FA and MA) to the positively charged surface. Notably, in pH 4 phosphate the maleate again appears to be the dominant adsorbate, despite coinciding with significant selectivity to FA, whereas the other electrolytes all have features from both FA and MA. It is thus seen how different pH conditions can lead to significantly different product selectivities via differences in the displacement of furfural and bound carboxylates that steer preferred reaction pathways.

Conclusions

In summary, we have investigated furfural oxidation on Pt/C electrocatalysts under a variety of reaction conditions, including changes in pH, supporting anion, reactant concentration, and potential. The largest changes in selectivity were found to result from changes in operating potential. The associated change in surface chemistry from Pt to

PtO_x results in a shift from FA as the dominant product to a mixture of primarily HFN and MA, consistent with previous results performed at differential conversion. There are thus apparently no significant secondary oxidation products except for CO_2. It was also observed that over time the cell currents decay asymptotically due to the accumulation of FA and MA as inhibitors, rather than reaching the endpoint in conversion or due to electrode fouling. This was confirmed by recycling studies that illustrated that activity losses were reversible.

Only mild effects were observed upon changing concentration, with higher concentration slightly increasing the selectivity toward FA. On the other hand, increasing the pH from 1 to 4 resulted in higher FA yields. In all cases, higher pH also diminished selectivity to HFN, speculatively due to a greater affinity for carboxylic acids that can be deprotonated at higher pH. Changing the supporting anion from perchlorate to phosphate resulted in significant selectivity changes as well; these changes were dependent on pH and potential. At low potential (0.9 V vs RHE), H_3PO_4 (pH 1) resulted in higher selectivity to MA, whereas NaH_2PO_4 (pH 4) resulted in a preference for FA. This is suggested to relate to steric hindrance of flat-lying furfural binding modes by a high coverage of specifically-adsorbed H_2PO_4–. These findings point to the potential success of introducing alternative binding agents to the surface of platinum to change selectivity. Alternatively, active separations might be instituted to suppress the product inhibition caused by carboxylic acid products.

Experimental Section

Materials: All solutions were prepared using ultrapure (UP) deionized water (>18.2 MΩ cm, Millipore). Furfural (99%, Sigma-Aldrich) was purified by vacuum distillation and then stored at −70 °C until needed in experiments. All other reagents and standards were used as delivered: Suprapure perchloric acid (70%, Millipore Sigma), sodium perchlorate (Laboratory Grade Fischer Scientific), Suprapure sulfuric acid (96%, Millipore Sigma), Nafion 117, sodium perchlorate monohydrate (Fischer Scientific), platinum wire, plate and gauze (Alfa Aesar), 2-furoic acid (98%, Sigma-Aldrich), 2(5H)-furanone (96%, Sigma-Aldrich), 5-hydroxy-2(5H)-furanone (96%, Enamine LLC), maleic acid (99%, Sigma-Aldrich), argon (UHP, AirGas), 2-propanol (HPLC Grade, Sigma-Aldrich), 40% Pt on carbon (XC-72 support, Fuel Cell Store grade, Fuel Cell Store), Nafion (5% w/w, Sigma-Aldrich), and carbon cloth (fuel cell store).

Cyclic Voltammetry: CVs were measured in a standard three electrode cell using a Gamry 3000 potentiostat. A flame polished platinum plate was used as a working electrode and a flame polished platinum mesh attached to a platinum wire was used as a counter electrode. A homemade Ag/AgCl electrode was used as a reference electrode; however, all potentials are reported against the reversible hydrogen electrode (RHE). Cyclic voltammograms were performed in electrolyte that was bubbled with Ar for at least 10 minutes before blanketing with Ar during measurements. The working electrode was broken in with 30 cycles (or until cyclic voltammograms were stable) from 0.05 V to 1.3 V at 150 mV/s. Following were 3 cycles at 20 mV/s taken over the same potential range to determine the electrochemical surface area (ECSA) assuming a stripping charge 210

μC/cm^2 for the hydrogen absorption region.[48] Uncompensated resistance was taken before each experiment and was typically < 5 Ω. All currents are reported with full iR-compensation, where the measurements were taken with 85% active iR-compensation.

Electrolysis Experiments: Chronoamperometry experiments were performed in a typical H-cell with a 13 mL working and 15 mL counter volume (to maintain an equal electrolyte height between two different sized H-cell halves). A Nafion 117 membrane sealed with a Viton O-ring was used to separate the working and counter electrodes. To create the working electrode, 4 carbon cloth flags were cut to approximately 4 cm x 0.75 cm. Next, 6 x 75 μL aliquots of a Pt/C ink deposited were near the bottom of each flag, with drying in a vacuum oven at 70°C between depositions. The Pt/C ink consisted of 5 mg of 40% Pt/C per mL of a 76% water, 24% IPA mixture. 20 μL of 5% Nafion per mL of solution was also added. This ink was sonicated for at least 1 hour before and between every deposition. The electrode flags were strung from the top of the cell with a platinum wire that was also used as the lead. A Pt gauze was used as the counter electrode, and a homemade Ag/AgCl reference electrode, calibrated against an RHE, was used. Four solutions were used for electrolysis: 0.1 M $HClO_4$ and 1.3 M H_3PO_4 for pH 1, and 0.0001 M $HClO_4$ + 0.0999 M $NaClO_4$ and 1 M NaH_2PO_4 for pH 4. The solution was bubbled for 10 minutes with argon before starting, then blanketed with argon for the duration. An identical break-in and ECSA measurement procedure was used as described for CVs above. Chronoamperometric electrolysis then consisted of holding constant operating potentials between 0.9 V and 1.3 V. Uncompensated resistance was measured before each experiment and was typically < 2 Ω. All currents are reported with iR-compensation,

with the measurements taken at 85% iR-compensation. During chronoamperometry, 0.5 mL samples were taken for HPLC analysis at 0.5, 1, 2, 4, 7, 10, and 22 hours using polytetrafluoroethylene (PTFE) tubing and a syringe. Full calculation details for selectivities and faradaic efficiencies over the course of sampling (accounting for loss in volume from withdrawn fluid) can be found in the Supporting Information.

Chemical Analysis: Reaction products were analyzed using an Advion 2000 HPLC equipped with a UV diode array detector (DAD) as well as an Advion Expression Compact Mass Spectrometer-S series. The mobile phase was 40 mM sulfuric acid with a flow rate of 0.4 mL/min. Aliquots of 100 µL were injected into a 300 mm × 6.5 mm sulfonated polystyrene gel column (Hi-Plex H, Agilent) at 60 °C. Two samples were taken from both the working and counter chambers before being diluted 50x and 2x (to ensure linear detector response in different concentration regimes) with HPLC grade water at each time point. The autosampler temperature was set to 4 °C to minimize degradation reactions prior to sampling. During MS studies, 0.01% formic acid was used in isocratic flow, maintaining the flow rate at 0.4 mL/min. The first 10 minutes of flow diverted to waste to avoid introduction of corrosive electrolyte to the ion source. Products were identified using atmospheric pressure chemical ionization, alternating positive (3 µA) and negative (25 µA) ionization modes. The source gas (N_2) was set to a temperature of 300 °C and flowed at 4 L/min. The ionized vapor impinged onto a capillary inlet at 200 °C with a capillary voltage of 120 V. Products were quantified via the UV DAD using the following wavelengths: MA, HFA, FN and HFN (210 nm), and FA (250 nm). External calibration curves were produced from standard solutions made in the working electrolyte.

For species without a commercial standard to characterize with chromatography (HFA), additional analysis was carried out by ^{1}H nuclear magnetic resonance (NMR) spectroscopy (Bruker AVANCE-III 400 MHz) in accordance with our previous work where we first identified HFA as a product[36]. In a typical experiment, 400 µL of collected electrolyte was combined with 100 µL of D_2O along with sodium trimethylsilylpropanesulfonate (DSS) (508 µM) as an internal standard. To prevent sample degradation, NMR experiments were conducted promptly after sampling and sample preparation. NMR results were then combined with 210 nm wavelength UV HPLC data, to create a calibration curve for HFA, which was then used for all other experiments.

A subset of samples was examined using 2D COSY experiments to aid in the structure assignment and HPLC calibration curve calculation. These samples were extracted from an electrolysis experiment performed in D_2O (with 0.1 M $HClO_4$ as the supporting electrolyte) to achieve a cleaner spectrum. More details on NMR structure identification are included in Ref [36].

ATR-SEIRA spectroscopy: The SEIRA-active platinum electrode was made by electroless deposition on a 'Specialized 1' SEIRAS optimized silicon wafer (IRUBIS) using a well-established plating method[49, 50]. The Si wafer was polished with a series of progressively finer aluminum slurries, ending at 0.05µm. The wafer was then thoroughly rinsed before being sequentially sonicated upright for 20 min in a 50:50 mixture of UP water and 2-propanol, and then pure UP water. The untextured surface of the Si surface was then subjected to a 2 min 1.0 mM $PdCl_2$ in 1% w/w HF etch to deposit a Pd adhesion layer[51]. A solution of 0.02 M $Pt(NH_3)_6$ was then prepared by combining a stoichiometric

amount of H_2PtCl_6 in 1 M NH_3 in water. This was kept as a stock solution and stored for a maximum of two weeks in the refrigerator. From this stock, a solution of 0.0036 M $Pt(NH_3)_6$, 0.09 M NH_3 and 0.0108 M hydrazine was prepared in UP water, and a droplet was applied to the wafer (preheated to 60ºC) for 3 minutes. A second droplet was then applied without rinsing and left for another 3 minutes. The resultant Pt film was then cycled 50 times between 0.05 V (vs. RHE) and 1.3 V (vs. RHE) at 50 mV/s. After initial cycling, the cell typically had an uncompensated resistance of 45-50 Ω and a roughness factor of ~5 found by hydrogen underpotential deposition, assuming 210 μC/cm^2.[48]

SEIRAS measurements were recorded using p-polarized light from a Nicolet 6700 FTIR equipped with a liquid nitrogen cooled MCT-A detector. A Jackfish J1W spectroelectrochemical cell attached to a Pike Veemax III accessory with an incident angle of 35º was mounted in the spectrometer. All measurements were taken with a resolution of 4 cm^{-1}. A Gamry 1010 potentiostat was used for all electrochemical measurements. Pt gauze (Alfa Aesar) attached to a platinum wire (Alfa Aesar) was used as a counter electrode, and a homemade Ag/AgCl reference electrode was used; however, all potentials are reported vs. RHE. All experiments were performed in the indicated N_2 purged electrolyte in UP H_2O. To account for changes in spectral features associated with Pt oxide formation on the surface, a potential-based background subtraction of spectra in pure electrolyte solution was used for all measurements unless otherwise stated.

Acknowledgements

The authors acknowledge support from the Department of Energy (DE-SC0023322). In addition, the authors would like to thank Adam Baz, Taylor Spivey, Yuval Fishler, Todd Whittaker, Nathanael Ramos, Dr. Francisco W.S. Lucas, and Dr. Yaran Zhao for assistance running experiments.

Conflict of Interest

The authors declare no competing financial interests.

Keywords:

Oxidation, Electro-oxidation, Furfural, Platinum, ATR-SEIRAS,

References

[1] F. W. S. Lucas, R. G. Grim, S. A. Tacey, C. A. Downes, J. Hasse, A. M. Roman, C. A. Farberow, J. A. Schaidle, A. Holewinski, *ACS Energy Lett.* **2021**, 1205–1270.

[2] J. P. Lemmon, *Nature* **2015**, *525*, 447–449.

[3] N. Tripathi, C. D. Hills, R. S. Singh, C. J. Atkinson, *Npj Clim. Atmospheric Sci.* **2019**, *2*, DOI 10.1038/s41612-019-0093-5.

[4] A. J. Ragauskas, C. K. Williams, B. H. Davison, G. Britovsek, J. Cairney, C. A. Eckert, W. J. Frederick, J. P. Hallett, D. J. Leak, C. L. Liotta, J. R. Mielenz, R. Murphy, R. Templer, T. Tschaplinski, *Science* **2006**, *311*, 484–489.

[5] J. C. Serrano-Ruiz, R. Luque, A. Sepúlveda-Escribano, *Chem. Soc. Rev.* **2011**, *40*, 5266–5281.

[6] K. M. Nicholas, Ed. , *Selective Catalysis for Renewable Feedstocks and Chemicals*, Springer International Publishing, Cham, **2014**.

[7] S. Nanda, D.-V. N. Vo, P. K. Sarangi, Eds. , *Biorefinery of Alternative Resources: Targeting Green Fuels and Platform Chemicals*, Springer Singapore, Singapore, **2020**.

[8] S. Kang, J. Fu, G. Zhang, *Renew. Sustain. Energy Rev.* **2018**, *94*, 340–362.

[9] Q. Li, J. Xing, *Production of 1,4-Diacids (Succinic, Fumaric, and Malic) from Biomass*, **2017**.

[10] W. Mu, H. Ben, A. Ragauskas, Y. Deng, *Bioenergy Res.* **2013**, *6*, 1183–1204.

[11] F. X. Collard, J. Blin, *Renew. Sustain. Energy Rev.* **2014**, *38*, 594–608.

[12] Y. C. Lin, G. W. Huber, *Energy Environ. Sci.* **2009**, *2*, 68–80.

[13] P. Rachamontree, T. Douzou, K. Cheenkachorn, M. Sriariyanun, K. Rattanaporn, *Appl. Sci. Eng. Prog.* **2020**, *13*, 3–10.

[14] L. Du, Y. Shao, J. Sun, G. Yin, C. Du, Y. Wang, *Catal. Sci. Technol.* **2018**, *8*, 3216–3232.

[15] K. Li, Y. Sun, *Chem. – Eur. J.* **2018**, *24*, 18258–18270.

[16] J. Carneiro, E. Nikolla, *Annu. Rev. Chem. Biomol. Eng.* **2019**, *10*, 85–104.

[17] R. Mariscal, M. Ojeda, *Energy Environ. Sci.* **2016**, *9*, 1144–1189.

[18] P. Nilges, U. Schröder, *Energy Environ. Sci.* **2013**, *6*, 2925–2931.

[19] J. P. Lange, E. Van Der Heide, J. Van Buijtenen, R. Price, *ChemSusChem* **2012**, *5*, 150–166.

[20] J. D. Holladay JE, Bozell JJ, White JF, **2004**, *II*.

[21] M. S. Mettler, D. G. Vlachos, P. J. Dauenhauer, *Energy Environ. Sci.* **2012**, *5*, 7797–7809.

[22] Y. Kwon, K. J. P. Schouten, J. C. Van Der Waal, E. De Jong, M. T. M. Koper, *ACS Catal.* **2016**, *6*, 6704–6717.

[23] R. Wojcieszak, F. Santarelli, S. Paul, F. Dumeignil, F. Cavani, R. V Gonçalves, *Sustain. Chem. Process.* **2015**, *3*, 9.

[24] A. Corma Canos, S. Iborra, A. Velty, *Chem. Rev.* **2007**, *107*, 2411–2502.

[25] G. R. Dick, A. D. Frankhouser, A. Banerjee, M. W. Kanan, *Green Chem.* **2017**, *19*, 2966–2972.

[26] K. A. P. Payne, S. A. Marshall, K. Fisher, M. J. Cliff, D. M. Cannas, C. Yan, D. J. Heyes, D. A. Parker, I. Larrosa, D. Leys, *ACS Catal.* **2019**, *9*, 2854–2865.

[27] K. Gupta, R. K. Rai, S. K. Singh, *ChemCatChem* **2018**, *10*, 2326–2349.

[28] M. Douthwaite, X. Huang, S. Iqbal, P. J. Miedziak, G. L. Brett, S. A. Kondrat, J. K. Edwards, M. Sankar, D. W. Knight, D. Bethell, G. J. Hutchings, *Catal. Sci. Technol.* **2017**, *7*, 5284–5293.

[29] N. Alonso-Fagúndez, I. Agirrezabal-Telleria, P. L. Arias, J. L. G. Fierro, R. Mariscal, M. L. Granados, *RSC Adv.* **2014**, *4*, 54960–54972.

[30] X. Li, W. Wan, S. Kattel, J. G. Chen, T. Wang, *J. Catal.* **2016**, *344*, 148–156.

[31] X. Li, J. Ko, Y. Zhang, *ChemSusChem* **2018**, *11*, 612–618.

[32] N. Alonso-Fagúndez, M. Ojeda, R. Mariscal, J. L. G. Fierro, M. López Granados, *J. Catal.* **2017**, *348*, 265–275.

[33] T. Soták, M. Hronec, M. Gál, E. Dobročka, J. Škriniarová, *Catal. Lett.* **2017**, *147*, 2714–2723.

[34] N. Araji, D. D. Madjinza, G. Chatel, A. Moores, F. Jérôme, K. De Oliveira Vigier, *Green Chem.* **2017**, *19*, 98–101.

[35] S. Shi, H. Guo, G. Yin, *Catal. Commun.* **2011**, *12*, 731–733.

[36] A. M. Román, J. C. Hasse, J. W. Medlin, A. Holewinski, *ACS Catal.* **2019**, *9*, 10305–10316.

[37] A. M. Román, N. Agrawal, J. C. Hasse, M. J. Janik, J. W. Medlin, A. Holewinski, *J. Catal.* **2020**, *391*, 327–335.

[38] L. O. Mark, N. Agrawal, A. M. Román, A. Holewinski, M. J. Janik, J. W. Medlin, *ACS Catal.* **2019**, *9*, 11360–11370.

[39] J. C. Hasse, N. Agrawal, M. J. Janik, A. Holewinski, *J. Phys. Chem. C* **2022**, acs.jpcc.2c01259.

[40] J. Y. Gui, D. A. Stern, F. Lu, A. T. Hubbard, *J. Electroanal. Chem.* **1991**, *305*, 37–55.

[41] G. A. Planes, E. Moran, J. L. Rodriguez, C. Barbero, E. Pastor, *Langmuir* **2003**, *19*, 8899–8906.

[42] R. M. Williams, S. H. Pang, J. W. Medlin, *J. Phys. Chem. C* **2014**, *118*, 27933–27943.

[43] L. O. Mark, A. H. Jenkins, H. Heinz, J. W. Medlin, *Surf. Sci.* **2018**, *677*, 333–340.

[44] S. H. Pang, A. M. Román, J. W. Medlin, *J. Phys. Chem. C* **2012**, *116*, 13654–13660.

[45] A. Gandini, M. N. Belgacem, *Prog. Polym. Sci. Oxf.* **1997**, *22*, 1203–1379.

[46] S. Ye, H. Kita, A. Aramata, *J. Electroanal. Chem.* **1992**, *333*, 299–312.

[47] R. Gisbert, G. García, M. T. M. Koper, *Electrochimica Acta* **2010**, *55*, 7961–7968.

[48] Y. Kwon, K. J. P. Schouten, M. T. M. Koper, *ChemCatChem* **2011**, *3*, 1176–1185.

[49] A. Miki, S. Ye, T. Senzaki, M. Osawa, *J. Electroanal. Chem.* **2004**, *563*, 23–31.

[50] C. D. Silva, G. Cabello, W. A. Christinelli, E. C. Pereira, A. Cuesta, *J. Electroanal. Chem.* **2017**, *800*, 25–31.

[51] A. Miki, S. Ye, M. Osawa, *Chem. Commun.* **2002**, 1500–1501.

TOC Entry:

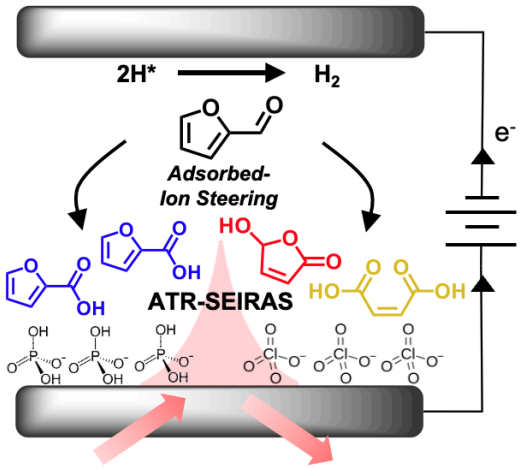

The effect of the reaction environment is examined for the electrochemical valorization of biomass-derived furfural using a series of electrolysis experiments and complementary spectroscopic observations from ATR-SEIRAS.